

Multifrequency Floquet Engineering of Magnon Polaritons

L. Hackner,^{1,2} A. R. Myatt,^{1,2} W. Wustmann,^{1,2} and N. J. Lambert^{1,2,*}

¹*Department of Physics, University of Otago, Dunedin, New Zealand*

²*Dodd-Walls Centre for Photonic and Quantum Technologies, Dunedin, New Zealand*

(Dated: May 8, 2026)

Floquet engineering of cavity magnon-polaritons by periodically modulating the magnon frequency has recently attracted much interest as a way to manipulate the energy spectrum of magnon-photon hybrid systems. However, modulating the frequency of magnons by a time-varying bias magnetic field can be challenging. We demonstrate cavity magnon-polariton Floquet engineering by modulating the microwave cavity frequency, allowing large modulation depth and bandwidth. We apply commensurate two-frequency Floquet modulations with the higher frequency at twice and three times the lower frequency, and demonstrate that the resulting spectrum depends on the relative amplitude and phase of the two drive tones. In comparison with single-frequency Floquet modulations, the spectrum has qualitatively different features; in particular, new anticrossings appear between previously uncoupled sidebands. Our platform offers an alternative way to manipulate Floquet quasi-energy levels in hybrid systems.

Cavity electromagnonic systems are a promising emerging platform for quantum technologies^{1,2}. In these hybrid devices, a magnetically ordered material exhibiting well-defined magnetostatic resonances is embedded in an electromagnetic cavity or resonator such that the supported magnons can exchange energy with the photons. If the mode overlap between the two excitations is sufficiently large, the coupling rate between the two exceeds the dissipation rates in the system, and the strong coupling regime is reached³⁻⁶. Judicious selection of cavity or magnon host material can allow ultrastrong coupling to be observed^{7,8}. The resulting hybrid excitations are termed magnon-polaritons, and demonstrations of hybrid devices based on magnons have included strong coupling between magnons and qubits⁹, strong coupling between spatially separated magnon populations¹⁰, and non-reciprocal devices^{11,12}. They have been proposed as a candidate platform for a variety of quantum technologies including coherent transducers¹³⁻¹⁶ and quantum memories¹⁷⁻¹⁹.

There has been significant recent interest in temporal periodic modulation of the parameters of cavity electromagnonic systems, resulting in changes in their dynamics. This powerful technique, termed Floquet engineering, introduces controllable quasienergy levels into the system's spectrum. Despite the significant experimental difficulties associated with rapid tuning of the magnon modes, there have been a number of demonstrations of Floquet physics in magnonic systems²⁰. The technique has been applied to a range of problems, such as the engineering of magnon dark modes²¹, controllable magnon-magnon coupling²², and the generation of entangled states^{23,24}. The new energy bands created are also of more fundamental interest; they have non-trivial topological properties²⁵⁻²⁷, and have been demonstrated to exhibit novel phases²⁷. Recently, the difficulty of achiev-

ing large frequency modulations was tackled by using a resonantly-enhanced drive field²⁸.

However, there remain significant experimental challenges associated with rapid tuning of the magnon modes. A time-varying magnetic field of a relatively large amplitude must be applied over the volume of the magnetic material, preferably via a coil or antenna with a low inductance and a flat frequency response over a broad range. Furthermore, the field should be as uniform as possible to avoid inhomogeneous broadening, of and coupling between, different magnetostatic modes^{29,30}. Here, we avoid the difficulties of modulating the magnon frequency by instead employing a rapidly tunable microwave resonator. Whilst the symmetry between the magnon and photon modes in the equations describing the system means that the underlying physics remains the same, our approach allows for large amplitudes and frequencies of modulation, and furthermore arbitrary and precisely controlled modulation waveforms can be applied. We use this approach to study dual-frequency Floquet driving of the hybrid system, focusing primarily on the case where one frequency is twice the other, and the case where one frequency is three times the other.

Our device (Fig. 1(a)) comprises a loop of coplanar waveguide on a low-loss printed circuit board (PCB) (Rogers 4003C) with an embedded amplifier (Mini-Circuits YSF-322+) and an in-phase/quadrature (IQ) demodulator (Marki Microwave MMIQ-0205HSM-2). We also add a backwards-wave stripline directional coupler (-16dB coupling, Mini-Circuits SCBD-16-63HP+) to the loop to provide coupling to a feedline. Resonant modes occur when the propagating microwave field undergoes a $2n\pi$ (where n is an integer) phase shift during one round trip of the loop. The phase shift has a controllable component due to the IQ demodulator; applying carefully calibrated voltages to the I and Q ports of the demodulator allows high bandwidth control of the frequency of the modes. The amplitude of the propagating wave is also dependent on the I and Q voltages, thus allow-

* Contact author: nicholas.lambert@otago.ac.nz

ing control over the total energy loss per round trip and hence the internal loss rate of the cavity mode. (Here we keep the internal loss of the mode constant throughout.)

A polished yttrium iron garnet (YIG) sphere³¹ of diameter 1 mm is inserted between the centre conductor and the ground plane of the waveguide loop such that the magnetic field component of the microwave field through the sphere is normal to the PCB. YIG is a common material for hybrid magnonic devices due to its high spin density and low loss, helping to reach the strong coupling regime between magnons and photons; a spherical geometry gives a well understood family of modes^{32,33}.

To calibrate the I and Q voltages required for a particular set of cavity parameters, the magnon population is detuned from the cavity by applying a magnetic field such that the magnon frequency $\omega_m/2\pi$ is above 4 GHz. We apply static voltages from an arbitrary waveform generator (AWG) and measure the transmission spectrum of the feedline from port 1 to port 2 (S21) using a vector network analyser (VNA), as in Fig. 1(a). We observe an absorption dip due to the cavity resonance, and determine the centre frequency and linewidth from a Lorentzian fit. By iteratively tuning the applied voltages until the centre frequency and linewidth of the resonance matches a particular target frequency and loss rate, we find the trajectory in (I,Q) voltage space corresponding to frequency modulation with constant internal loss rate.

We then use the AWG to apply waveforms corresponding to a single tone Floquet drive such that the time-varying angular frequency of the microwave mode is given by $\omega(t) = \omega_c + a\sin(\Omega t)$, where Ω and a are the Floquet drive frequency and drive amplitude, respectively. In Fig. 1(b) we show $|S_{21}|$ for the modulated cavity (with the magnon frequency still far detuned from the cavity frequency) as a function of $\Omega/2\pi$, with $\omega_c/2\pi = 2.615$ GHz and $a/2\pi = 70$ MHz. Sidebands appear at $\omega_c \pm n\Omega$, with integer n . Furthermore, we find that the n th sideband disappears at the zeros of the Bessel function $J_n(a/\Omega)$ (top axis) as expected²⁰, confirming that our I and Q voltage calibration still applies with higher frequency drives and is not bandwidth limited in any way.

When the applied magnetic field is such that the magnon frequency is similar to the photon frequency, the excitations of the system become hybridized magnon-polaritons. We probe the spectrum of the hybrid system by measuring S21. We begin by tuning the cavity frequency to 2.17 GHz. In all the following experiments we fix the internal loss rate of the cavity to be $2\pi \times 2$ MHz, and we determine the external loss rate (set by the coupling of the directional coupler) to be $2\pi \times (1.60 \pm 0.05)$ MHz. In order to tune the magnon mode frequency through the cavity frequency, we sweep an in-plane magnetic field H_{dc} from 64 mT to 73.7 mT. We observe an anticrossing between the spatially uniform (Kittel) magnon mode supported by the YIG and photons in the cavity (Fig. 1(c)), demonstrating that the two are in the strong coupling regime. By fitting the eigenmodes

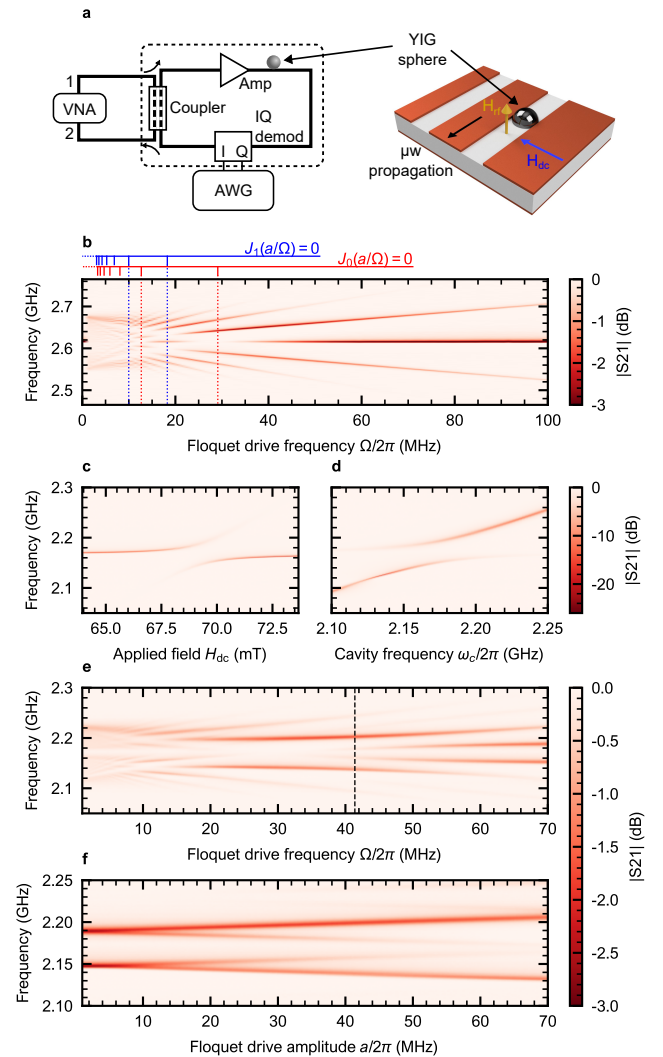


FIG. 1. Experimental setup and device characterisation. (a) Schematic the hybrid magnonic device comprising a microwave ring resonator with gain (Amp) and phase control (IQ), and an embedded YIG sphere (right). A vector network analyser (VNA) measures the transmission (S21) of a feedline, and an arbitrary waveform generator (AWG) allows the frequency of the cavity modes to be modulated. (b) $|S_{21}|$ of uncoupled cavity mode spectrum under single tone frequency modulation as function of drive frequency $\Omega/2\pi$, with $\omega_c/2\pi = 2.615$ GHz, showing sidebands with minima coincident with Bessel function zeros (top axis, dotted lines.) (c) $|S_{21}|$ as a function of applied magnetic field, with $\omega_c/2\pi = 2.17$ GHz, showing a magnon-photon anticrossing of size $2g/2\pi = 41.6$ MHz. (d) $|S_{21}|$ as a function of cavity frequency ω_c , with magnetic field H_{dc} fixed at 69 mT, again showing an anticrossing. (e) $|S_{21}|$ as a function of Floquet drive frequency $\Omega/2\pi$, with $\omega_c/2\pi = \omega_m/2\pi = 2.17$ GHz and $a/2\pi = 50$ MHz. (f) $|S_{21}|$ of feedline as a function of probe frequency and Floquet drive amplitude, with $\omega_c/2\pi = \omega_m/2\pi = 2.17$ GHz, and $\Omega/2\pi = 41.4$ MHz $= 2g/2\pi$, corresponding to the dashed line in panel (e).

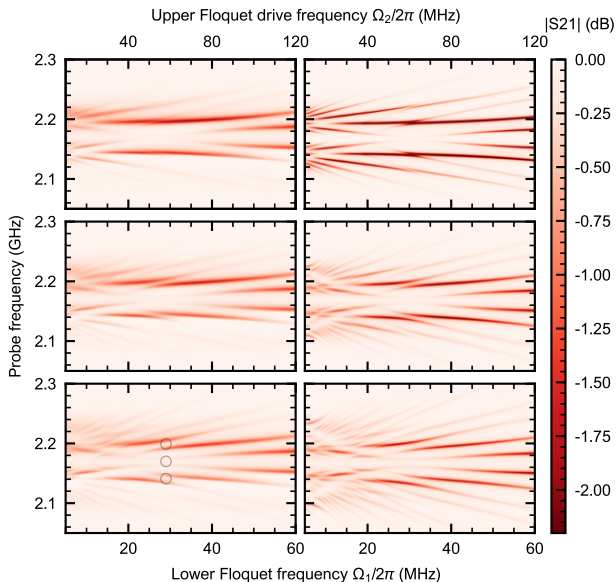


FIG. 2. $|S_{21}|$ of feedline for two-frequency cavity modulation with $\Omega_2 = 2\Omega_1$, $a_1/2\pi = 40$ MHz, and $\phi = 0$. $\Omega_1/2\pi$ is stepped from 5 MHz to 60 MHz. Rows from top to bottom correspond to $a_2/2\pi = 10$ MHz, $a_2/2\pi = 25$ MHz, $a_2/2\pi = 40$ MHz. Left column shows experimental data; right column – input-output theory (see main text).

of two coupled oscillators to the observed anticrossing, we determine a coupling rate of $g/2\pi = 20.7$ MHz. We next fix the applied field at 69 mT, resulting in a bare magnon frequency of 2.17 GHz, and use the tunability of our microwave cavity to sweep the photon frequency from 2.1 GHz to 2.25 GHz. We again see an anticrossing between the modes (Fig. 1(d)), and find a minimum mode separation of $2g/2\pi = 2 \times 20.5$ MHz, in reasonable agreement with the previous measurement.

We now set the cavity mode centre frequency to $\omega_c/2\pi = 2.17$ GHz, and apply a magnetic field of 69 mT, thereby tuning the microwave cavity and magnon frequencies to be equal. The excitations of the hybrid system are then two magnon-polariton modes of angular frequencies $\omega_{\pm} = \omega_c \pm g$. Using the AWG we apply waveforms to the IQ demodulator corresponding to a single tone Floquet drive such that the time-varying angular frequency of the microwave mode is again given by $\omega(t) = \omega_c + a \sin(\Omega t)$. We measure S_{21} as before.

In Fig. 1(e) we show $|S_{21}|$ as a function of Floquet frequency $\Omega/2\pi$ and probe frequency, with the amplitude of the Floquet drive fixed at $a/2\pi = 50$ MHz. Sidebands are seen on both magnon-polariton branches, spaced at integer multiples of $\Omega/2\pi$ from the underlying modes. At the point where $\Omega/2\pi = 41.4$ MHz $= 2g/2\pi$, we see an anticrossing between the first upper (lower) sideband of the lower (upper) magnon-polariton branch ($\omega_{\mp} \pm \Omega$) and the upper (lower) magnon-polariton branch (ω_{\pm}). We also see a family of anticrossings between higher order modes at lower Floquet frequencies Ω , following the rule that for finite coupling sizes Δn must be odd. For example, the

sideband of order -1 of the upper branch ($\omega_+ - \Omega$) and the sideband of order $+1$ of the lower branch ($\omega_- + \Omega$) do not anticross with each other.

We next study the dependence of the size of the anticrossing between ω_{\pm} and $\omega_{\mp} \pm \Omega$ on the amplitude of the Floquet drive, a . We fix $\Omega/2\pi = 41.4$ MHz $= 2g/2\pi$ (dashed line in Fig. 1(e)), which is the low power limit of the position of the anticrossing between these modes. In Fig. 1(f) we show $|S_{21}|$ for this value of Ω as a function of Floquet amplitude $a/2\pi$ and probe frequency. We see that the coupling between sideband and magnon-polaritons increases with increasing a .

The quasienergy level spectrum measured so far, while extended to higher drive amplitudes, is consistent with previous measurements on cavity magnon-polariton systems in which the Floquet drive was applied to the magnon population²⁰. However, the visibility of the modes in S_{21} measurements is different here to that seen in Ref. [20]. We ascribe this to the fact that in our case the photon mode, through which the behaviour of the system is probed, is modulated rather than the magnon mode. This leads to destructive interference between the $n - 1$ sideband of the upper magnon-polariton branch, and the $n + 1$ sideband of the lower magnon-polariton branch, rendering the mode dark.

We now move beyond single-tone driving to multi-

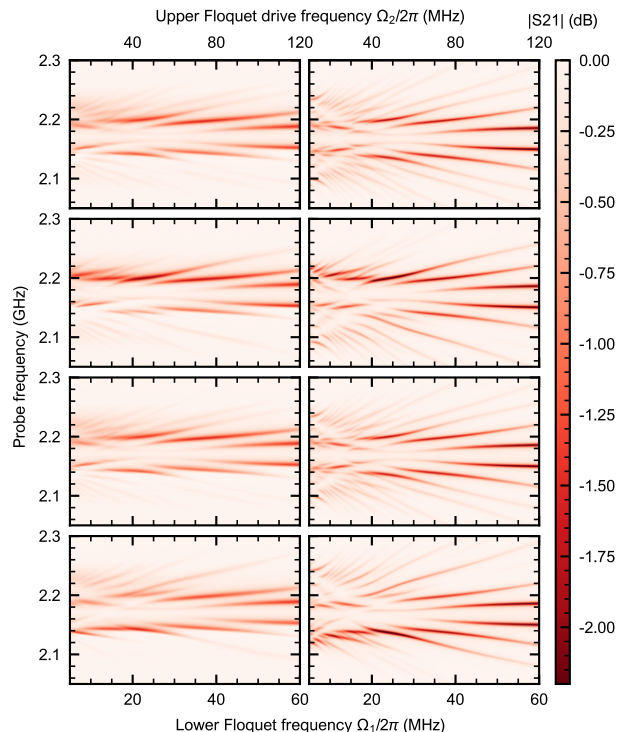


FIG. 3. $|S_{21}|$ of feedline for two-frequency cavity modulation with $\Omega_2 = 2\Omega_1$, $a_1/2\pi = 35$ MHz, and $a_2/2\pi = 40$ MHz. $\Omega_1/2\pi$ is stepped from 5 MHz to 60 MHz. Rows from top to bottom correspond to $\phi = 0$, $\phi = \pi/2$, $\phi = \pi$, $\phi = 3\pi/2$. Left column shows experimental data; right column – input-output theory.

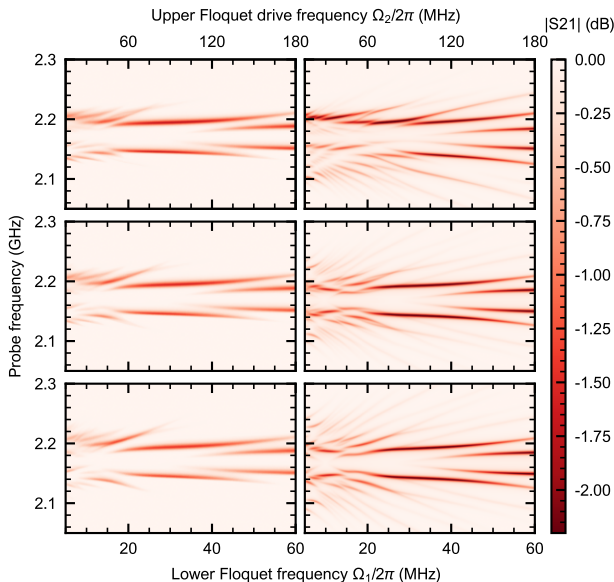


FIG. 4. $|S_{21}|$ of feedline for two-frequency cavity modulation with $\Omega_2 = 3\Omega_1$, $a_1/2\pi = 32.5$ MHz, and $\phi = 0$. $\Omega_1/2\pi$ is stepped from 5 MHz to 60 MHz. Rows from top to bottom correspond to $a_2/2\pi = 20$ MHz, $a_2/2\pi = 30$ MHz, $a_2/2\pi = 40$ MHz. Left column shows experimental data; right column – input-output theory.

frequency modulation. We apply commensurate two-frequency Floquet drives such that $\omega(t) = \omega_c + a_1 \sin(\Omega_1 t) + a_2 \sin(\Omega_2 t + \phi)$, where $\Omega_2 = m\Omega_1$ and m is integer and small. We start by applying waveforms for which $m = 2$. In the left column of Fig. 2 we show $|S_{21}|$ as a function of Ω_1 , with $\Omega_2 = 2\Omega_1$ (shown on the upper x -axes), for $a_1/2\pi = 40$ MHz, $\phi = 0$, and (panels from top to bottom) $a_2/2\pi = \{10$ MHz, 25 MHz, 40 MHz $\}$. The multi-tone driving introduces modifications to the quasi-mode spectrum; in particular anticrossings are now introduced between sidebands for which Δn is even. Most noticeably, anticrossings open between the $\omega_+ - \Omega$ and $\omega_- + \Omega$ sidebands, the ω_+ mode and $\omega_- + 2\Omega$ sideband, and the ω_- mode and $\omega_+ - 2\Omega$ sideband; these are highlighted with grey circles in the lower left panel of Fig. 2. Within this range of second Floquet amplitude a_2 , the anticrossings dependent on the upper frequency increase in size with increasing a_2 . Conversely, the size of those anticrossings which do not rely on the presence of the drive at Ω_2 , such as those at $\Omega_1 \approx 47$ MHz, are not influenced by a_2 in its measured range.

The time-varying system can be modeled using the Floquet matrix formalism^{34,35} for the time-periodic Hamiltonian

$$H(t) = H_0 + V_{\text{dr}}(t) \quad (1)$$

$$\hbar^{-1}H_0 = \omega_c c^\dagger c + \omega_m m^\dagger m + g c^\dagger m + g^* m^\dagger c \quad (2)$$

$$\hbar^{-1}V_{\text{dr}}(t) = c^\dagger (a_1 \sin(\Omega_1 t) + a_2 \sin(\Omega_2 t + \phi)). \quad (3)$$

By expanding this in terms of its harmonics we write it in matrix form. The n th 2×2 diagonal block is of the

form

$$\begin{bmatrix} \omega_c + n\Omega_1 & g \\ g & \omega_m + n\Omega_1 \end{bmatrix} \quad (4)$$

(where in our experiments $\omega_c = \omega_m$) and describes the underlying magnon-polariton system. In our calculations we truncate the matrix at sidebands of order $n = \pm 8$. The multi-frequency Floquet coupling is modelled with off-diagonal blocks of the form

$$\begin{bmatrix} \pm \frac{1}{2} i a_1 & 0 \\ 0 & 0 \end{bmatrix} \quad (5)$$

between diagonal blocks n and $n \pm 1$ corresponding to the coupling due to Ω_1 , and of form

$$\begin{bmatrix} \pm \frac{1}{2} i a_2 e^{\mp i \phi} & 0 \\ 0 & 0 \end{bmatrix} \quad (6)$$

between blocks n and $n \pm m$ corresponding to the coupling due to Ω_2 . Comparison to experimental results is carried out using cavity input-output theory³⁶, with the input mode coupling to the $n = 0$ cavity mode. In the right column of Fig. 2 we show $|S_{21}|$ calculated using this model, with the same parameters as the experimental results in the left column, and the loss rate of the magnon modes⁶ set to $2\pi \times 5$ MHz. We find excellent agreement between the two.

The inclusion of a second drive tone introduces another degree of freedom in addition to the modulation depth – the relative phase between the two tones. In Fig. 3 (left column) we fix $a_1/2\pi = 32.5$ MHz and $a_2/2\pi = 40$ MHz. The phase ϕ is varied within each column in steps of $\pi/2$, starting with $\phi = 0$ in the uppermost panels. At phase differences of $\phi = \pi/2$ and $\phi = 3\pi/2$ we observe asymmetric sidebands, such that the visibilities are different between upper and lower sidebands with positive and negative n . This is due to each sideband being generated by multiple paths characterised by Bessel functions of different order n ; for example a sideband at $\omega_- + 2\Omega_1$ has a contribution from the second order sideband due to Ω_1 , of strength $J_2(a_1/\Omega_1)$, and a contribution from the first order sideband due to Ω_2 , of strength $J_1(a_2/\Omega_2)$. The phase shift between the two drive frequencies results in either positive or negative interference between alternative sideband generation paths involving different signs of n , and hence different signs of the corresponding Bessel functions^{37,38}. Our results are again in good agreement with multi-frequency Floquet theory and input-output theory (Fig. 3, right column).

Finally, we apply waveforms such that $\Omega_2 = 3\Omega_1$ with Ω_2 up to 180 MHz, fix $\phi = 0$, and again measure S_{21} (Fig. 4). Further structure is introduced to the spectrum. We note in particular, the condition that Δn must be odd for finite coupling between quasi-energy levels is restored; for example, level crossings are introduced between $\omega_+ - \Omega$ and $\omega_- + \Omega$. This is due to the coupling Hamiltonian once more having only odd terms when expanded in terms of Bessel functions. Our results are well

described by Floquet theory as before (Fig. 4, right column).

In conclusion, we have demonstrated Floquet engineering in a cavity magnon-polariton system in which the photon frequency rather than the magnon frequency is modulated. This gives us access to large depth and frequencies of modulation, allowing multifrequency Floquet drives to be applied. We demonstrate that, as well as the drive amplitudes, the relative phase between the drives affects the resulting quasi-energy spectrum, and leads to asymmetric sidebands. Our results are described well using a Floquet Hamiltonian and input-output theory. Our device architecture is a versatile platform for the study of physics in which cavity mode parameters including both frequency and lifetime³⁹ are varied in time.

ACKNOWLEDGMENTS

WW and NJL are supported by *Quantum Technologies Aotearoa*, a research program funded by the New Zealand Ministry of Business, Innovation and Employment, contract number UOO2347. NJL acknowledges funding from Royal Society of New Zealand Marsden Grant no. 24-UOO-153.

AUTHOR CONTRIBUTIONS

NJL conceptualized and supervised the experiment. LH performed experimental measurements and data analysis. ARM and WW carried out theoretical analysis and contributed to data analysis. WW and NJL prepared the manuscript.

-
- [1] D. Lachance-Quirion, Y. Tabuchi, A. Gloppe, K. Usami, and Y. Nakamura, Hybrid quantum systems based on magnonics, *Applied Physics Express* **12**, 070101 (2019).
- [2] B. Zare Rameshti, S. Viola Kusminskiy, J. A. Haigh, K. Usami, D. Lachance-Quirion, Y. Nakamura, C.-M. Hu, H. X. Tang, G. E. W. Bauer, and Y. M. Blanter, Cavity magnonics, *Physics Reports Cavity Magnonics*, **979**, 1 (2022).
- [3] M. Goryachev, W. G. Farr, D. L. Creedon, Y. Fan, M. Kostylev, and M. E. Tobar, High-Cooperativity Cavity QED with Magnons at Microwave Frequencies, *Physical Review Applied* **2**, 054002 (2014).
- [4] Y. Tabuchi, S. Ishino, T. Ishikawa, R. Yamazaki, K. Usami, and Y. Nakamura, Hybridizing Ferromagnetic Magnons and Microwave Photons in the Quantum Limit, *Physical Review Letters* **113**, 083603 (2014).
- [5] X. Zhang, C.-L. Zou, L. Jiang, and H. X. Tang, Strongly Coupled Magnons and Cavity Microwave Photons, *Physical Review Letters* **113**, 156401 (2014).
- [6] N. J. Lambert, J. A. Haigh, and A. J. Ferguson, Identification of spin wave modes in yttrium iron garnet strongly coupled to a co-axial cavity, *Journal of Applied Physics* **117**, 053910 (2015).
- [7] J. Bourhill, N. Kostylev, M. Goryachev, D. L. Creedon, and M. E. Tobar, Ultrahigh cooperativity interactions between magnons and resonant photons in a YIG sphere, *Physical Review B* **93**, 144420 (2016).
- [8] J. R. Everts, G. G. King, N. J. Lambert, S. Kocsis, S. Rogge, and J. J. Longdell, Ultrastrong coupling between a microwave resonator and antiferromagnetic resonances of rare-earth ion spins, *Physical Review B* **101**, 214414 (2020).
- [9] Y. Tabuchi, S. Ishino, A. Noguchi, T. Ishikawa, R. Yamazaki, K. Usami, and Y. Nakamura, Coherent coupling between a ferromagnetic magnon and a superconducting qubit, *Science* **349**, 405 (2015).
- [10] N. J. Lambert, J. A. Haigh, S. Langenfeld, A. C. Doherty, and A. J. Ferguson, Cavity-mediated coherent coupling of magnetic moments, *Physical Review A* **93**, 021803 (2016).
- [11] Y.-P. Wang, J. W. Rao, Y. Yang, P.-C. Xu, Y. S. Gui, B. M. Yao, J. Q. You, and C.-M. Hu, Nonreciprocity and Unidirectional Invisibility in Cavity Magnonics, *Physical Review Letters* **123**, 127202 (2019).
- [12] X. Zhang, A. Galda, X. Han, D. Jin, and V. M. Vinokur, Broadband Nonreciprocity Enabled by Strong Coupling of Magnons and Microwave Photons, *Physical Review Applied* **13**, 044039 (2020).
- [13] R. Hisatomi, A. Osada, Y. Tabuchi, T. Ishikawa, A. Noguchi, R. Yamazaki, K. Usami, and Y. Nakamura, Bidirectional conversion between microwave and light via ferromagnetic magnons, *Phys. Rev. B* **93**, 174427 (2016).
- [14] A. Osada, R. Hisatomi, A. Noguchi, Y. Tabuchi, R. Yamazaki, K. Usami, M. Sadgrove, R. Yalla, M. Nomura, and Y. Nakamura, Cavity optomagnonics with spin-orbit coupled photons, *Phys. Rev. Lett.* **116**, 223601 (2016).
- [15] X. Zhang, N. Zhu, C.-L. Zou, and H. X. Tang, Optomagnonic whispering gallery microresonators, *Phys. Rev. Lett.* **117**, 123605 (2016).
- [16] N. Zhu, X. Zhang, X. Han, C.-L. Zou, C. Zhong, C.-H. Wang, L. Jiang, and H. X. Tang, Waveguide cavity optomagnonics for microwave-to-optics conversion, *Optica* **7**, 1291 (2020).
- [17] K. R. Ferguson, S. E. Beavan, J. J. Longdell, and M. J. Sellars, Generation of Light with Multimode Time-Delayed Entanglement Using Storage in a Solid-State Spin-Wave Quantum Memory, *Physical Review Letters* **117**, 020501 (2016).
- [18] H. Tanji, S. Ghosh, J. Simon, B. Bloom, and V. Vuletić, Heralded Single-Magnon Quantum Memory for Photon Polarization States, *Physical Review Letters* **103**, 043601 (2009).
- [19] X. Zhang, C.-L. Zou, N. Zhu, F. Marquardt, L. Jiang, and H. X. Tang, Magnon dark modes and gradient memory, *Nature Communications* **6**, 8914 (2015).
- [20] J. Xu, C. Zhong, X. Han, D. Jin, L. Jiang, and X. Zhang, Floquet Cavity Electromagnonics, *Physical Review Letters* **125**, 237201 (2020).
- [21] A. Pishevar, Z. Wang, Y. Zhu, Y. Jiang, Z. Yan, F. Li, J. M. Jornet, J.-M. Hu, L. Jiang, and X. Zhang, On-demand magnon resonance isolation in cavity magnonics,

- Physical Review Applied **23**, 024053 (2025).
- [22] S. Heidarpour, A. Abdolali, and B. Z. Rameshti, Floquet-driven control of indirect magnon coupling in microwave cavities, *Physical Review B* **112**, 024432 (2025).
- [23] X. Zhu, R. Xia, and L. Xu, Floquet-engineering magnonic NOON states with performance improved by soft quantum control, *Quantum Information Processing* **22**, 454 (2023).
- [24] S.-f. Qi and J. Jing, Floquet generation of a magnonic NOON state, *Physical Review A* **107**, 013702 (2023).
- [25] Q.-H. Chen, F.-J. Huang, Y.-P. Fu, and H. Su, Floquet no-go theorem and engineering topological magnons, *Physical Review B* **111**, 064426 (2025).
- [26] J. Minguzzi, Z. Zhu, K. Sandholzer, A.-S. Walter, K. Viebahn, and T. Esslinger, Topological Pumping in a Floquet-Bloch Band, *Physical Review Letters* **129**, 053201 (2022).
- [27] S. Olin and W.-C. Lee, Topological phase transition in the commensurate multifrequency Floquet Su-Schrieffer-Heeger model, *Physical Review B* **107**, 094310 (2023).
- [28] A. Pishevvar, Z. Yan, Z. Wang, Y. Jiang, Y. Huang, J. M. Jornet, L. Jiang, and X. Zhang, Resonance-enhanced Floquet cavity electromagnonics, *Physical Review Applied* **24**, 014026 (2025).
- [29] E. Schlömann, Inhomogeneous Broadening of Ferromagnetic Resonance Lines, *Physical Review* **182**, 632 (1969).
- [30] J. A. Haigh, N. J. Lambert, S. Sharma, Y. M. Blanter, G. E. W. Bauer, and A. J. Ramsay, Selection rules for cavity-enhanced Brillouin light scattering from magnetostatic modes, *Phys. Rev. B* **97**, 214423 (2018).
- [31] www.ferrisphere.com.
- [32] L. R. Walker, Magnetostatic modes in ferromagnetic resonance, *Phys. Rev.* **105**, 390 (1957).
- [33] P. Fletcher, I. H. Solt, and R. Bell, Identification of the magnetostatic modes of ferrimagnetic resonant spheres, *Phys. Rev.* **114**, 739 (1959).
- [34] A. N. Poertner and J. D. D. Martin, Validity of many-mode Floquet theory with commensurate frequencies, *Physical Review A* **101**, 032116 (2020).
- [35] J. H. Shirley, Solution of the Schrödinger Equation with a Hamiltonian Periodic in Time, *Physical Review* **138**, B979 (1965).
- [36] C. W. Gardiner and M. J. Collett, Input and output in damped quantum systems: Quantum stochastic differential equations and the master equation, *Physical Review A* **31**, 3761 (1985).
- [37] G. R. Janik, C. B. Carlisle, and T. F. Gallagher, Two-tone frequency-modulation spectroscopy, *JOSA B* **3**, 1070 (1986).
- [38] J. G. Proakis and M. Salehi, *Communication Systems Engineering* (Prentice Hall, Upper Saddle River, New Jersey, 2002) 2nd ed., p. 109.
- [39] N. J. Lambert, A. Schumer, J. J. Longdell, S. Rotter, and H. G. L. Schwefel, Coherent control of magnon-polaritons using an exceptional point, *Nature Physics* **21**, 1570 (2025).